Journal of the Korean Physical Society, Vol. 73, No. 5, September 2018, pp. 638∼648

Coherent Energy Transfer Dynamics and Photoluminescence of Coupled Quantum Dots: Fully Analytical Approach

Kwang Jun Ahn*
Department of Energy Systems Research/Department of Physics, Ajou University, Suwon 16499, Korea

(Received 2 July 2018)

We theoretically studied coherent excitation energy transfer between self-growth semiconductor quantum dots (QDs) by solving Heisenberg's equations of motion for density matrix elements in second quantization regime. In a local excitation condition where only one QD electron is optically excited by the pump laser field, coherent excitation energy transfer to the other QD electron can be achieved through Coulomb (Förster) and electron-photon (radiation field) interactions. We calculated three diagonal and one off-diagonal Coulomb coupling constants, which are responsible for the biexcitonic frequency renormalization and the coherent energy transfer between QDs, respectively, and radiation field coupling coefficients by using electron and hole wave functions derived from eight-band kp-theorem, whose validity has already been tested by comparison with experiment. In linear optical regime where the occupation densities of electrons at higher energy level are negligibly small, we could successfully derive fully analytical behaviors of temporal dynamics of the interband polarizations and level occupation densities of both QDs by using Hartree-Fock approximation (HFA), in eventual, the stationary photoluminescence of the coupled QDs in an analytical form. Additionally, the validity of the HFA was examined by comparing the numerical results with those obtained from the exact correlation expansion model for different values of the pump field intensity.

PACS numbers: 78.67.Hc, 78.60.Lc, 42.50.Ex
Keywords: Cohernt energy transfer, Coupled quantum dots, Förster interaction
DOI: 10.3938/jkps.73.638

I. INTRODUCTION

Semiconductor quantum dots (QDs) are one of intensively studied low-dimensional materials. Atom-like discrete energy distribution easily controlled by the spatial dimension of QDs [1] and relatively small decay rate [2,3] promote semiconductor QDs to a highly promising candidate for constructing logic devices for quantum computing [4–11].

Several types of quantum bit (qubit) were introduced for QDs. For example, a linear superposition of off- and on-state of exciton (Coulomb-coupled electron-hole pair) [5] or two energetically different states of exciton [12], denoted respectively as $|a\rangle$ and $|b\rangle$, is suggested for single qubit [5]. A new entangled state (for instance $|ab\rangle$) can be generated by a gate processing of two qubits via interactions between them.

The electric dipole interaction is known to be a fundamental coupling between two atomic light emitters and discriminated into longitudinal Förster interaction [13–16] and the transversal radiation field coupling [17–21].

In order to build highly entangled states for quantum gate operation, the coherent excitation energy of a donor QD must be successfully transfered to an acceptor QD through the interactions. However, the energy transfer rate by the dipole interaction between two QDs is strongly influenced by dephasing processes such as the electron-longitudinal acoustic phonon interaction [2,22–27] and the radiative decay [28,29], because externally induced coherent excitations in the donor QD can be completely dephased by them during the energy transfer. Therefore, understanding the interplay between the interaction for coherent energy transfer and dephasing processes is the key ingredient for realizing quantum logic gate based on QDs. Even in the case that dephasing processes are stronger than the dipole interaction, several solutions have been introduced; entanglement accomplished only by the binding energy of biexciton in coupled QDs [8], enhanced electron-photon coupling through positioning QDs in high-Q cavities [4,7,30,31] or by using surface plasmon resonance of metals [32,33].

In this study, as a basic building block for entangled qubits, two Coulomb- and radiation field-coupled QDs are theoretically investigated. At first, we perform Taylor expansion of $1/|\mathbf{r}-\mathbf{r}'|$ in Coulomb interaction, where $\mathbf{r}$ and $\mathbf{r}'$ are two position vectors of electrons in each QD [6], at around lattice vectors and the center of QD,

*E-mail: kjahn@ajou.ac.kr

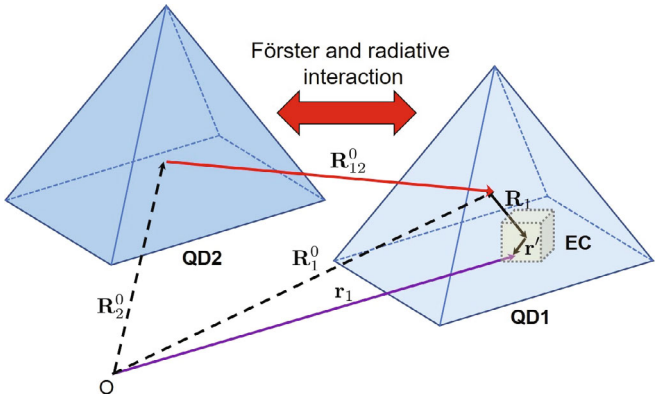

Fig. 1. (Color online) Schematic presentation of the considered coupled QD system. The spatial vector $\mathbf{r}$ is divided into a vector pointing the center of the n^{th} QD, $\mathbf{R}_n^0$, the lattice vector $\mathbf{R}_n$, and a small extension vector $\mathbf{r}'$ within elementary cell.

respectively. Then, we obtain three diagonal coupling matrix elements related to biexcitonic shifts and one off-diagonal (Förster) element which is responsible for the longitudinal coherent energy transfer. All coupling matrix elements are numerically determined as a function of the distance between two identical QDs by using the wave functions of electron and hole in self growth QDs with pyramidal shape [34]. The transverse radiation field coupling coefficients are obtained in a similar way.

Next, we derive Heisenberg's quantum kinetic equations of motion for the electronic density matrix elements within the frame of 2nd quantization. In order to systematically study the different coherent energy transfer processes including dephasing, we consider local excitation situation, where only one QD electron is optically pumped by the laser field and its coherence is transferred to the other QD electron through Förster and radiation field interaction. In weak excitation condition where the electronic occupation density of the energetically higher level is negligibly small compared to that of the lower energy level, fully analytical solutions for the interband coherences and upper level electronic densities of both QDs can be derived within the Hartree-Fock approximation (HFA). Furthermore, photoluminescence (PL) spectrum of the coupled QD system can be obtained as an analytical form. We discussed also the validity and break-down of the HFA as a function of the pump laser intensity by comparing the numerical results with those of the exact solution (full correlation expansion).

II. HAMILTONIAN AND OBSERVABLES

In Fig. 1, spatial configuration of a coupled semiconductor QDs is schematically illustrated. Two identical QDs with pyramidal shape are assumed to be positioned at $\mathbf{r}_1$ and $\mathbf{r}_2$. The distance between the two QDs is defined as $R_0 = |\mathbf{r}_1 - \mathbf{r}_2|$. In this studies, we focus only single electron dynamics in each QD, and the interdot tunneling of electrons (the transition of an electron from one QD to the other) is not considered. Additionally, we take only the energetically lowest two levels of the electron ($\lambda = v, c$) into consideration as a model system for strongly confined QDs. By 2nd-quantizing electrons, the electronic field $\psi(\mathbf{r})$ is expressed by a product of the eigenstate $\xi_\lambda(\mathbf{r})$ of the confinement potential and the periodic Bloch function $u_\lambda(\mathbf{r})$ of the n^{th} QD:

$$\psi(\mathbf{r}) = \sum_{\lambda,n} \varphi_{\lambda n}(\mathbf{r}) a_{\lambda n} = \sum_{\lambda,n} \xi_{\lambda n}(\mathbf{r}) u_\lambda(\mathbf{r}) a_{\lambda n}, \quad (1)$$

where $a_{\lambda n}(a_{\lambda n}^\dagger)$ is the annihilation (creation) operator for the electron in state $|\lambda\rangle$ of the n^{th} QD.

For two interacting QD electrons, the Hamiltonian is given as

$$\hat{\mathbf{H}} = \hat{\mathbf{H}}_0 + \hat{\mathbf{H}}_{\text{c}} + \hat{\mathbf{H}}_{\text{ep}} + \hat{\mathbf{H}}_{\text{e-EM}}, \quad (2)$$

where the Hamiltonian for free kinetic energies of quantum confined Bloch electrons in effective mass approximation and free space photons are

$$\hat{\mathbf{H}}_0 = \hat{\mathbf{H}}_{\text{el}} + \hat{\mathbf{H}}_{\text{pt}} = \sum_{\lambda,n} \epsilon_{\lambda n} a_{\lambda n}^\dagger a_{\lambda n} + \sum_{\mathbf{k},j} \hbar\nu_k c_{\mathbf{k}j}^\dagger c_{\mathbf{k}j}, \quad (3)$$

In Eq. (3), $c_{\mathbf{k}j}(c_{\mathbf{k}j}^\dagger)$ denotes the annihilation (creation) operators of a photon with wave vector $\mathbf{k}$ for two orthogonal polarization directions j. The Coulomb interaction between the electrons is expressed by the Hamiltonian:

$$\hat{\mathbf{H}}_{\text{c}} = \sum_{\substack{\lambda_1\cdots\lambda_4 \\ n_1\cdots n_4}} V_{\lambda_1\lambda_2\lambda_3\lambda_4}^{n_1 n_2 n_3 n_4} a_{\lambda_1 n_1}^\dagger a_{\lambda_2 n_2}^\dagger a_{\lambda_4 n_4} a_{\lambda_3 n_3}, \quad (4)$$

where $V_{\lambda_1\lambda_2\lambda_3\lambda_4}^{n_1 n_2 n_3 n_4}$ are Coulomb coupling matrix elements. Their explicit forms are presented in the following subsection.

The transversal coherent energy transfer between two QD electrons and the self-energy renormalization including the radiative decay of individual electrons are caused by the electron-photon interaction. The corresponding Hamiltonian is known as

$$\hat{\mathbf{H}}_{\text{ep}} = -i\hbar \sum_{\lambda,\mu,n,\mathbf{k},j} g_n(kj) a_{\lambda n}^\dagger a_{\mu n} \left\{ c_{\mathbf{k}j} e^{i\mathbf{k}\cdot\mathbf{R}_n^0} - c_{\mathbf{k}j}^\dagger e^{-i\mathbf{k}\cdot\mathbf{R}_n^0} \right\},$$

$$g_n(kj) = \mathbf{d}_n \cdot \boldsymbol{\varepsilon}_j(\mathbf{k}) \sqrt{\frac{\omega_k}{2\epsilon_0 \hbar V}} \langle\mu|\nu\rangle,$$

$$\mathbf{d}_n = e_0 \int_{\text{ec}} \mathrm{d}^3\mathrm{r}' u_{\lambda n}^*(\mathbf{r}') \mathbf{r}' u_{\mu n}(\mathbf{r}'), \quad (5)$$

where $g_n(kj)$ is the coupling matrix element of the electron in the n^{th} QD to photons [35]. In $g_n(kj)$, $\boldsymbol{\varepsilon}_j(\mathbf{k})$ denotes the unit vector of the polarization satisfying the transversal property of bulk photons ($\mathbf{k} \cdot \boldsymbol{\varepsilon}_j(\mathbf{k}) = 0, j = 1, 2$), $\mathbf{d}_n$ the atomic dipole moment of the n^{th}

QD, and V the quantization volume. On account of the much smaller spatial dimension of the considered QD ($\sim$ 30 nm), compared to the wavelength of light corresponding to the gap energy ($\omega_g = 1.4$ eV $\sim$ 600 nm), we can safely assume that the electric field amplitude within QDs is uniform and the form factor of the electron-photon interaction is solely decided by $\langle\mu|\nu\rangle$.

The electrons optically pumped by a classical coherent laser field is expressed by the Hamiltonian:

$$\hat{\mathbf{H}}_{\text{e-EM}} = -\sum_{\lambda,\mu,n} \mathbf{d}_n \cdot \int \mathrm{d}^3\mathrm{R}\, \xi^*_{\lambda n}(\mathbf{R})\, \mathbf{E}(\mathbf{R}^0_n, t) \xi_{\mu n}(\mathbf{R}) a^\dagger_{\lambda n} a_{\mu n},$$
$$\mathbf{E}(\mathbf{R}^0_n, t) = \frac{1}{2}\left\{\mathbf{E}_e(\mathbf{R}^0_n, t) e^{i\omega_L t} + c.c.\right\}, \quad (6)$$

where ω_L is the center frequency of laser and $\mathbf{E}_e(\mathbf{r}, t)$ the slowly varying envelope of the laser field. In the local excitation regime, only one QD electron is assumed to be excited by the pump laser field. Such a situation can be implemented in experiments, for example, by guiding the pump laser field into a sharp near-field scanning optical microscope probe [36].

1. Coulomb coupling matrix elements

The Coulomb coupling matrix elements in the 2nd quantization regime is expressed as [37]

$$V^{n_1\cdots n_4}_{\lambda_1\cdots\lambda_4} = \frac{e^2}{8\pi\epsilon\epsilon_0} \iint \mathrm{d}r_1^3 \mathrm{d}r_2^3 \frac{1}{|\mathbf{r}_1 - \mathbf{r}_2|} \times \varphi^*_{\lambda_1 n_1}(\mathbf{r}_1)\varphi^*_{\lambda_2 n_2}(\mathbf{r}_2)\varphi_{\lambda_4 n_4}(\mathbf{r}_2)\varphi_{\lambda_3 n_3}(\mathbf{r}_1). \quad (7)$$

Dividing the spatial vector $\mathbf{r}_i$ $(i = 1, 2)$ into the lattice vectors $\mathbf{R}_n$ from the center of QD and $\mathbf{r}'$ defined within the elementary cell (see Fig. 1), $1/|\mathbf{r}_1 - \mathbf{r}_2|$ is replaced by a Taylor expansion derived at $\mathbf{R}_n$:

$$\frac{1}{|\mathbf{r}_1 - \mathbf{r}_2|} = \frac{1}{|\mathbf{R}_{lm}|} - \frac{\mathbf{R}_{lm}}{|\mathbf{R}_{lm}|^3}(\mathbf{r} + \mathbf{r}') + \frac{\mathbf{r}\cdot\mathbf{r}'}{|\mathbf{R}_{lm}|^3} - \frac{3}{|\mathbf{R}_{lm}|^5}\{\mathbf{r}\cdot\mathbf{R}_{lm}\}\{\mathbf{r}'\cdot\mathbf{R}_{lm}\}, \quad (8)$$

where $\mathbf{R}_{lm} = \mathbf{R}_l - \mathbf{R}_m$. By exchanging $\varphi_{\lambda n}$ with the product of $\xi_{\lambda n}(\mathbf{r}_n)$ and $u_\lambda(\mathbf{r}_n)$ (see Eq. (1)), we can get the diagonal ($\lambda_1 = \lambda_3$, $\lambda_2 = \lambda_4$) and the off-diagonal elements ($\lambda_1 \neq \lambda_3$, $\lambda_2 \neq \lambda_4$) of two coupled QD electrons ($n_1 = n_3$, $n_2 = n_4$), by virtue of the orthogonal properties of Bloch functions $u_\lambda(\mathbf{r}_n)$ in the elementary cell.

$$V^{n_1\cdots n_4}_{\lambda_1\cdots\lambda_4} = \frac{1}{8\pi\epsilon\epsilon_0}\sum_{l,m}\left[\frac{e_0^2}{|\mathbf{R}_{lm}|}|\xi_{\lambda_1 n_1}(\mathbf{R}_l)|^2|\xi_{\lambda_2 n_2}(\mathbf{R}_m)|^2\delta_{\lambda_1\lambda_3}\delta_{\lambda_2\lambda_4} + \frac{\mathbf{d}_{n_1}\cdot\mathbf{d}_{n_2}}{|\mathbf{R}_{lm}|^3} - \frac{3}{|\mathbf{R}_{lm}|^5}\{\mathbf{d}_{n_1}\cdot\mathbf{R}_{lm}\}\{\mathbf{d}_{n_2}\cdot\mathbf{R}_{lm}\} \times \xi^*_{\lambda_1 n_1}(\mathbf{R}_l)\xi^*_{\lambda_2 n_2}(\mathbf{R}_m)\xi_{\lambda_4 n_2}(\mathbf{R}_m)\xi_{\lambda_3 n_1}(\mathbf{R}_l)\right] \times \delta_{n_1 n_3}\delta_{n_2 n_4}. \quad (9)$$

Note that we ignored the second part of the right hand side in Eq. (8) due to the rotating wave approximation (RWA). Further expanding the first term at the center of the QD, we obtain three diagonal ($V^{1212}_{\lambda\mu\lambda\mu}$) and one off-diagonal ($V^{1212}_{vccv}$) coupling matrix elements between two same QDs:

$$V^{1212}_{vccv} = \frac{1}{8\pi\epsilon\epsilon_0}\sum_{l,m}\left\{\frac{\mathbf{d}_1\cdot\mathbf{d}_2}{|\mathbf{R}_{lm}|^3} - \frac{3}{|\mathbf{R}_{lm}|^5}\{\mathbf{d}_1\cdot\mathbf{R}_{lm}\}\{\mathbf{d}_2\cdot\mathbf{R}_{lm}\}\right\} \times \xi^*_{v1}(\mathbf{R}_l)\xi^*_{c2}(\mathbf{R}_m)\xi_{v2}(\mathbf{R}_m)\xi_{c1}(\mathbf{R}_l) =: V_F, \quad (10)$$

$$V^{1212}_{\lambda\mu\lambda\mu} = \frac{e_0^2}{8\pi\epsilon\epsilon_0}\sum_{l,m}\left\{\frac{\mathbf{R}^1_l\cdot\mathbf{R}^2_m}{|\mathbf{R}^0_{12}|^3} - \frac{3}{|\mathbf{R}^0_{12}|^5}(\mathbf{R}^1_l\cdot\mathbf{R}^2_m)(\mathbf{R}^2_l\cdot\mathbf{R}^1_m)\right\} \times |\xi_{\lambda 1}(\mathbf{R}_l)|^2|\xi_{\mu 2}(\mathbf{R}_m)|^2 =: V_{\lambda\mu} \quad (\lambda \neq \mu), \quad (11)$$

where $\mathbf{R}^0_{12} = \mathbf{R}^0_1 - \mathbf{R}^0_2$ and $\mathbf{R}^n_l = \mathbf{R}_l - \mathbf{R}^0_n$. While exciton's energy renormalization results from the diagonal elements $V_{\lambda\mu}$, the coherent excitation energy transfer between QD electrons, best known as Förster energy transfer [6], is caused by the off-diagonal element V_F.

In order to get the numerical values of all Coulomb coupling matrix elements, we adopted eight-band kp-theory wave functions of an electron in the conduction and a hole in the valence band, confined in a pyramidal shape of QD [38,39]. Their iso-surface plots can be found in Figs. 2(b) and (c), respectively. On account of the pyramidal shape of self-organized QDs, electron and the hole wave functions are strongly localized in specific regions. As a consequence, we obtain three different values of diagonal matrix elements (V_{vv}, V_{vc}, V_{cc}).

It is worthy to mention that the coupling matrix elements given by wave functions of highly symmetric spherical or cubic confinement can have a identical value or be zero on account of the wave functions' parities [6]. The electron and hole wave functions obtained from eight-band kp-theorem have been already validated through the binding energy of biexciton ($E^{XX} = 1.7$ meV) [40]. Independently, we tested

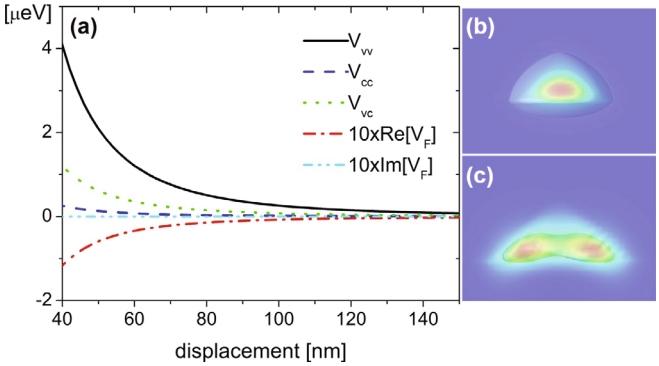

Fig. 2. (Color online) (a) Coulomb interaction matrix elements as a function of the displacement between two same QDs are calculated with the wave functions from eight-band kp-theorem. Iso-surface plots of (b) the electron in the conduction band and (c) the hole in the valence band.

V_{cc} which is defined as

$$V_{cc} = \frac{e_0^2}{4\pi\epsilon\epsilon_0}\int \mathrm{d}^3\mathrm{r}_1 \int \mathrm{d}^3\mathrm{r}_2 \frac{|\xi_c^*(\mathbf{r}_1)|^2|\xi_c^*(\mathbf{r}_2)|^2}{|\mathbf{r}_1-\mathbf{r}_2|}. \quad (12)$$

The numerically obtained value (24 meV) shows a fairly good agreement with experiment (23 meV) reported in [41].

Fig. 2 (a) shows numerical values of V_{vv}, V_{vc}, V_{cc}, and V_F as a function of the distance between two identical QDs. The spatial dimensions of the considered QD are $34\times34\times27$ nm^3. By taking into account the Coulomb interaction, the quantum kinetic equations of motion for the interband coherences (polarizations, $p_n = \langle a_{vn}^\dagger a_{cn}\rangle$) are additionally driven by

$$\partial_t p_1(t)\Big|_c = i\left\{\omega_F(\eta_{cvcc}-\eta_{vvcv}) + \omega_c\eta_{vccc} + \omega_b\eta_{vvvc}\right\}, \quad (13)$$

$$\partial_t p_2(t)\Big|_c = i\left\{\omega_F(\eta_{vccc}-\eta_{vvvc}) + \omega_b\eta_{vvcv} + \omega_c\eta_{cvcc}\right\}, \quad (14)$$

where $\omega_c = 2(V_{vc}-V_{cc})/\hbar$ and $\omega_b = 2(V_{vv}-V_{vc})/\hbar$ are the biexcitonic energy shifts and $\omega_F = 2V_F/\hbar$ is the Förster energy transfer rate. The single electron density matrix elements depend now on the two-electron coherence terms $\eta_{\kappa\lambda\mu\nu} := \langle a_{\kappa1}^\dagger a_{\lambda2}^\dagger a_{\mu2} a_{\nu1}\rangle$.

2. Radiation field coupling and self-energy correction

The coherent energy exchange between two QDs can occur by virtue of the transversal radiation field interaction. On the other hand, the renormalization of gap energy $\delta\omega$ and modified radiative lifetime $\tau = 1/\Gamma$ for QD electrons are originated from the same interaction [42].

Similar to the master equation approach [43], for example, the equations of motion for $\rho_{c1}(t) = \langle a_{c1}^\dagger a_{c1}\rangle$, the occupation density of the electron in the first QD at the upper energy level, and its hierarchically connected higher order terms by the interaction of electron with photon are given by

$$\partial_t\rho_{c1}(t) = 2\sum_{\mathbf{k},j}\mathrm{Re}\left[\tilde{g}_1(kj)\langle a_{v1}^\dagger a_{c1}c_{\mathbf{k}}\rangle - \tilde{g}_1^*(kj)\langle a_{v1}^\dagger a_{c1}c_{\mathbf{k}}^\dagger\rangle\right], \quad (15)$$

$$\partial_t\langle a_{v1}^\dagger a_{c1}c_{\mathbf{k}}^\dagger\rangle_e = \tilde{g}_1(kj)\rho_{c1}\,e^{i(\omega_1-\omega_k)t} + \tilde{g}_2(kj)\tilde{\eta}_{vcvc}\,e^{i(\omega_2-\omega_k)t}, \quad (16)$$

$$\partial_t\langle a_{c1}^\dagger a_{v1}c_{\mathbf{k}}\rangle_e = \tilde{g}_1^*(kj)\rho_{c1}\,e^{-i(\omega_1-\omega_k)t} + \tilde{g}_2^*(kj)\tilde{\eta}_{cvcv}\,e^{-i(\omega_2-\omega_k)t}, \quad (17)$$

$$\partial_t\langle a_{v1}^\dagger a_{c1}c_{\mathbf{k}}\rangle_e = \tilde{g}_2^*(kj)\tilde{\eta}_{vcvc}\,e^{i(\omega_2+\omega_k)t}, \quad (18)$$

$$\partial_t\langle a_{c1}^\dagger a_{v1}c_{\mathbf{k}}^\dagger\rangle_e = \tilde{g}_2(kj)\tilde{\eta}_{cvcv}\,e^{-i(\omega_2+\omega_k)t}, \quad (19)$$

where $\langle\cdot\rangle_e$ denote the slowly varying envelope of the expectation value $\langle\cdot\rangle$, $\tilde{g}_n(kj) = g_n(kj)e^{i\mathbf{k}\cdot\mathbf{R}_{12}^0}$, and $\tilde{\eta}_{vcvc} = \eta_{vcvc}\,e^{i(\omega_1-\omega_2)t} = \langle a_{v1}^\dagger a_{c2}^\dagger a_{v2}a_{c1}\rangle = \langle a_{c1}^\dagger a_{v2}^\dagger a_{c2}a_{v1}\rangle^*$. Eq. (15) can be rewritten by using formally integrated Eqs. (16) - (19) as

$$\begin{aligned}\partial_t\rho_1(t) = \sum_{\mathbf{k}}\int_{-\infty}^{t}\mathrm{d}t' \times\Big[&-\rho_{c1}(t')|g_1(k)|^2\left(e^{i(\omega_k-\omega_1)(t-t')}+e^{-i(\omega_k-\omega_1)(t-t')}\right)\\ &+\tilde{\eta}_{vcvc}(t')e^{-i\omega_{12}t}\left\{g_1(k)g_2^*(k)\,e^{-i(\omega_k+\omega_2)(t-t')} - g_1^*(k)g_2(k)\,e^{-i(\omega_k-\omega_2)(t-t')}\right\}\\ &+\tilde{\eta}_{cvcv}(t')e^{i\omega_{12}t}\left\{g_1^*(k)g_2(k)\,e^{i(\omega_k+\omega_2)(t-t')} - g_1(k)g_2^*(k)\,e^{-i(\omega_k-\omega_2)(t-t')}\right\}\Big].\end{aligned} \quad (20)$$

The self-energy correction including both the frequency normalization and the radiative decay Γ_1 is explained by the first part in the integrand. Assuming $\eta(t') \approx \eta(t)$ by Born-Markov approximation and replacing the sum over $\mathbf{k}$ with three-dimensional integration, we can simplify Eq. (20) as

$$\partial_t\rho_{c1}(t) = -\Gamma_1\rho_{c1}(t) - (\alpha_2 - i\beta_2)\tilde{\eta}_{vcvc}(t)\,e^{-i\omega_{12}t} - (\alpha_2 + i\beta_2^*)\tilde{\eta}_{cvcv}(t)e^{i\omega_{12}t}, \quad (21)$$

where $\omega_{12} = \omega_1 - \omega_2$ and the radiation field coupling coefficients α_n and β_n are defined as [18,43,44]

$$\alpha_n = \frac{|\mathbf{d}_n|^2\omega_n^3}{8\pi\epsilon_0\hbar c^3}\int_0^\pi \mathrm{d}\theta'\sin^3\theta' e^{i\frac{\omega_n}{c}R_{12}^0\cos\theta}, \quad (22)$$

$$\beta_n = \frac{|\mathbf{d}_n|^2}{8\pi\epsilon_0\hbar c^3}\int_0^\pi \mathrm{d}\theta'\sin^3\theta'\int_{-\infty}^{+\infty}\mathrm{d}\omega\frac{\omega^3 e^{i\frac{\omega}{c}R_{12}^0\cos\theta}}{\omega-\omega_n}, \quad (23)$$

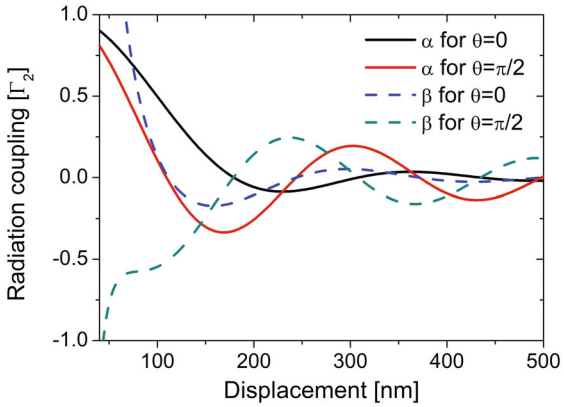

Fig. 3. (Color online) The real and imaginary part of the radiation field coupling coefficients α and β normalized by Γ_2 when the dipole moment of QD is oriented parallel ($\theta = 0$) or perpendicular ($\theta = \pi/2$) to $\mathbf{R}^0_{12}$.

$$\alpha_n + i\beta_n = \Gamma_{2n}\left\{\frac{h_2^{(2)}(y_n)}{2}(3\cos^2\theta - 1) + h_0^{(2)}(y_n)\right\}, \qquad y_n = \frac{\omega_n}{c}R^0_{12}, \quad (24)$$

where $\Gamma_{2n} = \Gamma_{1n}/2$, θ is the angle formed by $\mathbf{R}^0_{12}$ and the atomic dipole moment $\mathbf{d}_n$ of the QD index n, and $h_n^{(2)}(y)$ the second kind of spherical Hankel functions [45].

By using eight-band kp-theory wave functions, we calculate α and β and present them in Fig. 3 as a function of the distance between two QDs, where two different orientations of the dipole moment with respect to $\mathbf{R}^0_{12}$ are considered ($\theta = 0(\pi/2)$ for parallel (perpendicular) configuration). Compared to the radiative decay rate and the gap frequency of isolated QDs, those of the coupled QDs including α and β possess now the dependency on the distance between them.

The radiation field coupling yields additional terms in the equations of motion for $p_{1/2}$ as:

$$\partial_t p_1\Big|_{\rm ep} = -\Gamma_{12}p_1 + i\{\omega_b\eta_{vvvc} + \omega_c\eta_{vccc}\} + (i\tilde{\beta}_2^* + \alpha_2)(\eta_{cvcc} - \eta_{vvcv}), \quad (25)$$

$$\partial_t p_2\Big|_{\rm ep} = -\Gamma_{22}p_2 + i\{\omega_b\eta_{vvcv} + \omega_c\eta_{cvcc}\} + (i\tilde{\beta}_1 + \alpha_1)(\eta_{vccc} - \eta_{vvvc}), \quad (26)$$

where $\tilde{\beta}_n = 2V_F/\hbar + \beta_n$ is the effective coherent excitation energy transfer rate.

III. NUMERICAL SIMULATIONS AND ANALYSIS

With all Hamiltonian and coupling coefficients discussed in the previous section, temporal dynamics of density matrix elements are derived from Heisenberg's equation:

$$\frac{d}{dt}\langle O(t)\rangle = \frac{i}{\hbar}\langle[H,\ O]\rangle. \quad (27)$$

The observables mainly interested in this work are the interband coherences p_n, the upper level occupation densities ρ_{cn} of both QD electrons and the mean photon number $n_k = \langle c^\dagger_{\mathbf{k}}c_{\mathbf{k}}\rangle$. While the absorption spectrum is inferred from p_n [46], PL spectrum of the coupled QDs can be explained by ρ_{cn} and n_k [26].

In the previous section, we showed that single electron density matrix elements of both QDs are coupled via two-electron coherence terms $\eta_{\kappa\lambda\mu\nu}$ resulting from the Coulomb and radiation field coupling. Since the equations of purely electronic correlation expansions are closed, thus, they are exactly solvable numerically (see Appendix). On the contrary, photon-associated density matrix elements contain infinite hierarchy relations. We solve this problem by using Weisskopf-Wigner approximation. The detailed procedure can be found in [26, 47].

In order to investigate temporal dynamics of coherent energy transfer between two QDs, we use the Coulomb and radiation field coupling coefficients obtained for a fixed center-to-center distance between two QDs, $|\mathbf{R}^0_{12}| =$ 40 nm, the atomic dipole moment polarized in z-axis, $d = 0.3e_0$ nm, and the gap energy $\omega_g = 1.4$ eV as $V_{vv} = 4.08$ μeV, $V_{cc} = 0.26$ μeV, $V_{vc} = 1.2$ μeV, and $V_F = 0.12$ μeV. Additionally, we confine our focus mainly at coherent energy transfer dynamics between two same QDs, which yields $\omega_1 = \omega_2 = \omega_g$, $\Gamma_{11} = \Gamma_{21} = \Gamma_1 = 2\Gamma_2$, $\alpha_1 = \alpha_2 = \alpha$, and $\beta_1 = \beta_2 = \beta$. Because coherent excitation energy transfer can not occur between two synchronously excited identical QDs as discussed below, we study the energy exchange in local excitation condition (only one QD excited by the pump laser field).

1. HFA and coherent energy transfer dynamics

If the amplitude of the pump laser is sufficiently weak insomuch that the electronic occupation densities do not change significantly ($\rho_c(t) \approx 0$ and $\rho_v(t) \approx 1$), we can simplify the coupled set of equations by using HFA. In this circumstance, a two-electron coherence term is divided into a product of single electronic densities and a fully correlation term:

$$\langle a^\dagger_{\kappa 1}a^\dagger_{\lambda 2}a_{\mu 2}a_{\nu 1}\rangle = \langle a^\dagger_{\kappa 1}a_{\nu 1}\rangle\langle a^\dagger_{\lambda 2}a_{\mu 2}\rangle + \langle a^\dagger_{\kappa 1}a^\dagger_{\lambda 2}a_{\mu 2}a_{\nu 1}\rangle^c. \quad (28)$$

Here, we do not consider interdot transitions of electrons. $\langle a^\dagger_{\kappa 1}a^\dagger_{\lambda 2}a_{\mu 2}a_{\nu 1}\rangle^c$ is the contribution of two fully correlated electronic densities and, as can be seen below, becomes significant as the laser field intensity increases.

The contribution of correlation terms in linear optical regime can be estimated by investigating the equation for η^c_{vvvv}, which is the source term of other correlation terms:

$$\begin{aligned}\partial_t\eta^c_{vvvv} =&\partial_t\eta_{vvvv} - \rho_{v2}\,\partial_t\rho_{v1} - \rho_{v1}\,\partial_t\rho_{v2}\\ =&-2\mathrm{Im}[\omega_F\eta_{vcvc}](\rho_{v2}-\rho_{v1})\\ &-i\Omega(t)\left\{\eta^c_{cvvv}-\eta^c_{vvvc}+\eta^c_{vcvv}-\eta^c_{vvcv}\right\},\end{aligned} \tag{29}$$

where $\rho_{vn} = \langle a^\dagger_{vn}a_{vn}\rangle$ are the occupation densities of electrons at the lower energy level of QDs ($n = 1, 2$). Because $\rho_{v1} = \rho_{v2} \approx 1\ \forall t$ and other correlation terms except for η^c_{vvvv} are initially zero, no correlation of the two-electron coherence terms can be excited. More detailed discussion on validity and break-down of HFA can be found at Sec. III.3.

In HFA, single electronic densities p_n and ρ_{cn} of both QDs and, additionally, η_{vcvc} are sufficient to express dynamics of coherent excitation energy exchange:

$$\begin{aligned}\partial_t p_1(t) =&-(i\tilde{\omega}_1+\Gamma_2)p_1(t)-(i\tilde{\beta}_2+\alpha_2)p_2(t)\\ &+i\Omega_0\delta(t),\end{aligned} \tag{30}$$

$$\partial_t p_2(t) = -(i\tilde{\omega}_2+\Gamma_2)p_2(t)-(i\tilde{\beta}_1+\alpha_1)p_1(t), \tag{31}$$

$$\begin{aligned}\partial_t\rho_{c1}(t) =&-\Gamma_1\rho_{c1}(t)-\alpha_2(\eta_{vcvc}+\eta_{cvcv})\\ &+i\tilde{\beta}_2(\eta_{vcvc}-\eta_{cvcv}),\end{aligned} \tag{32}$$

$$\begin{aligned}\partial_t\rho_{c2}(t) =&-\Gamma_1\rho_{c2}(t)-\alpha_1(\eta_{vcvc}+\eta_{cvcv})\\ &-i\tilde{\beta}_1(\eta_{vcvc}-\eta_{cvcv}),\end{aligned} \tag{33}$$

$$\begin{aligned}\partial_t\eta_{vcvc} =&-\left\{i(\omega_1-\omega_2)-2\Gamma_2\right\}\eta_{vcvc}\\ &-(\alpha_1-i\tilde{\beta_1}^*)\rho_{c1}(t)-(\alpha_2+i\tilde{\beta_2}^*)\rho_{c2}(t),\end{aligned} \tag{34}$$

where $\tilde{\omega}_i = \omega_i - \omega_b$ and Ω_0 is the Rabi frequency.

Now, p_n and ρ_n are independent from each other and can be solved analytically. In the case that only one QD is optically excited by a very short pulse $\Omega_0\delta(t)$, the time-dependent interband coherences are obtained as

$$\begin{aligned}p_1(t) =&\frac{p_0}{2\Lambda}e^{-\frac{t}{2}\left[\Lambda+2\Gamma_2+i(\tilde{\omega}_1+\tilde{\omega}_2)\right]}\\ &\times\left\{\Lambda(1+e^{\Lambda t})-i(e^{\Lambda t}-1)(\tilde{\omega}_1-\tilde{\omega}_2)\right\},\end{aligned} \tag{35}$$

$$p_2(t) = \frac{p_0}{\Lambda}(\alpha_1+i\tilde{\beta}_1)e^{-\frac{t}{2}\left[\Lambda+2\Gamma_2+i(\tilde{\omega}_1+\tilde{\omega}_2)\right]}\left[1-e^{\Lambda t}\right], \tag{36}$$

where $\Lambda = \sqrt{4(\alpha_1+i\tilde{\beta}_1)(\alpha_2+i\tilde{\beta}^*_2)-(\tilde{\omega}_1-\tilde{\omega}_2)^2}$. Eqs. (32) - (34) can be analytically solved as well. By using the sum and the subtraction of both occupation densities $A := \rho_{c1}(t)+\rho_{c2}(t)$ and $B := \rho_{c1}(t)-\rho_{c2}(t)$, Eqs. (32) - (34) are reformulated as two homogeneous differential equations:

$$\partial_t^2\tilde{A} = -2\alpha(\dot{\tilde{\eta}}_{vcvc}+\dot{\tilde{\eta}}_{cvcv}) = 4\alpha^2\tilde{A}, \tag{37}$$

$$\partial_t^2\tilde{B} = 2i\beta(\dot{\tilde{\eta}}_{vcvc}-\dot{\tilde{\eta}}_{cvcv}) = -4\beta^2\tilde{B}, \tag{38}$$

where $\tilde{X} = Xe^{\Gamma_1 t}$ ($X = A,\ B$), $\tilde{\rho}_{cn} = \rho_{cn}e^{\Gamma_1 t}$. Then, we obtain the solutions as

$$\rho_{c1}(t) = \frac{\rho_0}{2}\left\{\cosh[2\alpha t]+\cos(2\tilde{\beta}t)\right\}e^{-\Gamma_1 t}, \tag{39}$$

$$\rho_{c2}(t) = \frac{\rho_0}{2}\left\{\cosh[2\alpha t]-\cos(2\tilde{\beta}t)\right\}e^{-\Gamma_1 t}, \tag{40}$$

where the initial conditions $\rho_{c1}(0) = \rho_0,\ \rho_{c2}(0) = 0$ for the local excitation are considered.

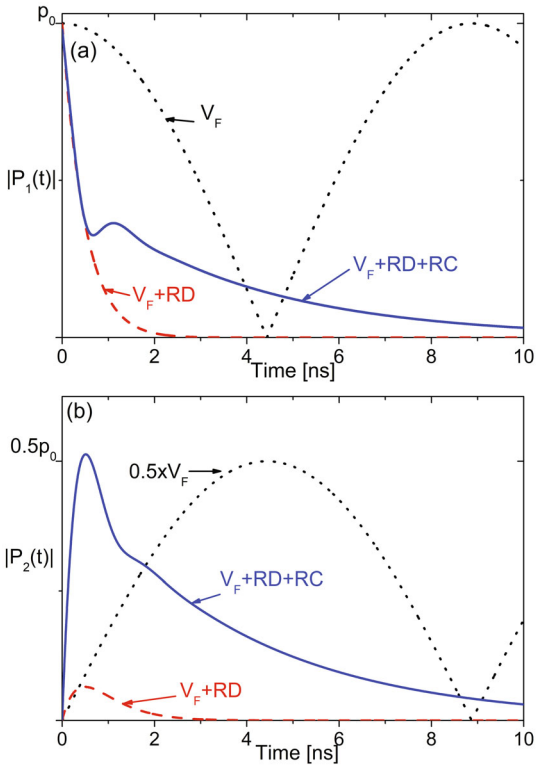

Fig. 4. (Color online) The coherent excitation energy transfer from the QD1 (a) to the QD2 (b) in the Förster coupling V_F, V_F and the radiative decay (RD), and V_F, RD and radiative coupling (RC), respectively.

Figure 4 presents temporal dynamics of the polarizations of the donor (Fig. 4(a)) and the acceptor QD (Fig. 4(b)), as three different coupling schemes are step by step included: 1) only Förster coupling (V_F, black dotted lines), 2) Förster coupling and the radiative decay (V_F+RD, red dashed lines), and 3) Förster and radiation couplings with the radiative decay (V_F+RD+RC, blue solid lines). From the spontaneous radiative decay rate corresponding to the Einstein coefficient, Γ_2 is approximately given as 0.9 μeV in homogeneous GaAs ($\epsilon_{\mathrm{GaAs}} = 12.5$). While a complete energy exchange between two QDs occurs within a few ns only by V_F, only a portion of the coherence energy is transferred to the acceptor when the radiative decay rate is included. Since $\Gamma_2 > \omega_F = 0.23$ μeV, the coherence induced at the donor QD is influenced and substantially dephased by Γ_2 before the energy transfer to the acceptor begins. When all interaction Hamiltonian (V_F+RD+RC) are included, the effective coherent energy transfer coefficients are given

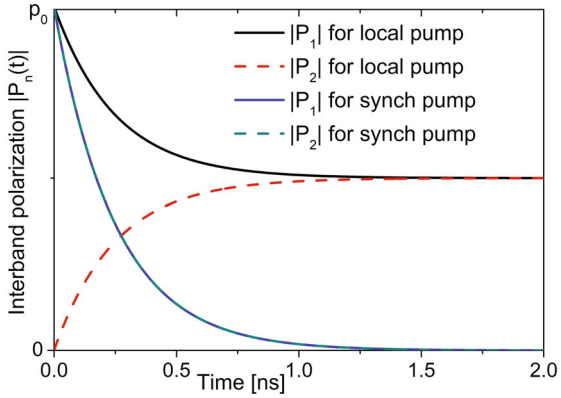

Fig. 5. (Color online) The polarizations in the synchronous excitation regime (both QDs are excited), in comparison to those in the local excitation condition(only one QD is excited).

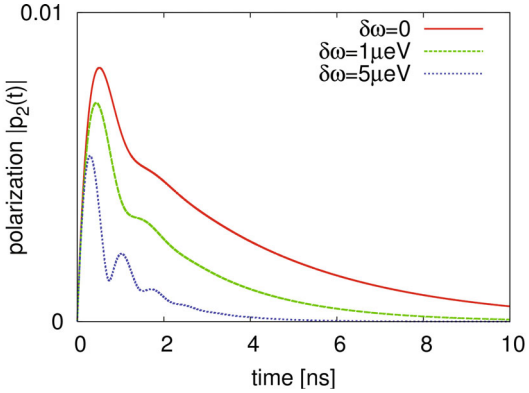

Fig. 6. (Color online) $|p_2(t)|$ of the acceptor QD induced by the coherent energy transfer from the donor QD for several energy differences ($\delta\omega = 0$, 1, 5 μeV). $|p_1(t)|$ is almost same as the resonant excitation (Fig. 4(a)) for three cases.

as $\alpha + i\tilde{\beta} \approx (0.72 - i1.35)$ μeV. We can find a weak but clear coherent energy exchange between two QDs.

Two cooperative optical behaviors called as super- and subradiance [18] can be reproduced in our theoretical approach. For $kR_{12}^0 \ll 1$, the real part of the radiation field coupling constants is approximated to $\alpha \approx \Gamma_2$ (see Fig. 3). For the initial condition ($p_2(t) = 0$), the interband coherences and occupation densities at the upper energy level of both QDs are written by

$$\begin{aligned} p_1(t) &= \frac{p_0}{2}(1 + e^{-2\Gamma_t})e^{-i\omega_g t}, \\ p_2(t) &= -\frac{p_0}{2}(1 - e^{-2\Gamma_t})e^{-i\omega_g t}, \end{aligned} \tag{41}$$

$$\begin{aligned} \rho_1(t) &= \frac{\rho_0}{4}(1 + 2e^{-\Gamma_1 t} + e^{-2\Gamma_1 t}), \\ \rho_2(t) &= \frac{\rho_0}{4}(1 - 2e^{-\Gamma_1 t} + e^{-2\Gamma_1 t}). \end{aligned} \tag{42}$$

$p_{1/2}$ and $\rho_{1/2}$ converge to the following stationary values, meaning that the spontaneous radiative decay of both QD electrons are blocked (subradiance):

$$\begin{aligned} \lim_{t\to\infty} p_1(t)e^{i\omega_g t} &= \lim_{t\to\infty} p_2(t)e^{i\omega_g t} = \frac{p_0}{2}, \\ \lim_{t\to\infty} \rho_1(t) &= \lim_{t\to\infty} \rho_2(t) = \frac{\rho_0}{4}. \end{aligned} \tag{43}$$

On the other hand, when the initial condition is changed to synchronous excitation ($p_2(0) = p_0,\ \rho_{c2}(0) = \rho_0$), $p_{1/2}$ and $\rho_{1/2}$ of both QDs show exactly same behavior: they decay with a two times larger decay constant (superradiance):

$$p_{1/2}(t) = p_0 e^{-2\Gamma_2 t}, \quad \rho_{1/2}(t) = \rho_0 e^{-2\Gamma_1 t}. \tag{44}$$

Two qualitatively different coherent energy transfer dynamics can be found in Fig. 5.

Finally, the coherent energy exchange dynamics between two energetically different QDs are simulated. Figure 6 shows $p_2(t)$ of the acceptor QD when the energy offset is given as $\delta\omega = 1$ μeV and 5 μeV. Compared to the case of resonant transfer ($\delta\omega = 0$ and Fig. 4), the reduced coherent energy transfer with enhanced oscillatory behavior of $p_2(t)$ can be found as $\delta\omega$ increases.

2. PL spectrum of coupled QD system

Fully analytical expressions of the interband coherences and electronic occupation densities in linear optical regime allow to write the stationary PL spectrum of the two coupled QDs as an analytical form as well. PL spectrum is obtained from stationary state of mean photon number $n_k(t)$ as a function of $\omega = c_0 k$ [26,47] where c_0 is speed of light in vacuum. $n_k(t)$ is calculated by solving the closed set of kinetic equations:

$$\begin{aligned} \partial_t n_k(t) &= \langle c_{\mathbf{k}}^\dagger c_{\mathbf{k}} \rangle \\ &= 2\mathrm{Re}[g_1(k)\langle a_{v1}^\dagger a_{c1} c_{\mathbf{k}}^\dagger \rangle + g_2(k) u_{\mathbf{k}}^*(\mathbf{R}_2^0)\langle a_{v2}^\dagger a_{c2} c_{\mathbf{k}}^\dagger \rangle], \end{aligned} \tag{45}$$

$$\begin{aligned} \partial_t \langle a_{v1}^\dagger a_{c1} c_{\mathbf{k}}^\dagger \rangle =& \Big\{ i(\nu_k - \omega_1) - \Gamma_2 \Big\} \langle a_{v1}^\dagger a_{c1} c_{\mathbf{k}}^\dagger \rangle \\ &+ g_1(k)\rho_{c1}(t) + g_2(k) u_{\mathbf{k}}(\mathbf{R}_2^0)\eta_{vcvc}, \end{aligned} \tag{46}$$

$$\begin{aligned} \partial_t \langle a_{v2}^\dagger a_{c2} c_{\mathbf{k}}^\dagger \rangle =& \Big\{ i(\nu_k - \omega_2) - \Gamma_2 \Big\} \langle a_{v2}^\dagger a_{c2} c_{\mathbf{k}}^\dagger \rangle \\ &+ g_2(k) u_{\mathbf{k}}(\mathbf{R}_2^0)\rho_{c2}(t) + g_1(k)\eta_{cvcv}, \end{aligned} \tag{47}$$

$$\begin{aligned} \partial_t \eta_{vcvc} =& -\Big\{ i\omega_{12} + 2\Gamma_2 \Big\} \eta_{vcvc} + (i\tilde{\beta}_1^* - \alpha_1)\rho_1(t) \\ &- (i\tilde{\beta}_2^* + \alpha_2)\rho_2(t), \end{aligned} \tag{48}$$

where $u_{\mathbf{k}}(\mathbf{R}_2^0) = \exp(i\mathbf{k}\cdot\mathbf{R}_2^0)$. For convenience, we assume that the donor and acceptor QDs (central points) are located at origin of the system coordinates and at $\mathbf{r} = \mathbf{R}_2^0$, respectively. Due to the broken radial symmetry of the two QD system with respect to the directions of atomic dipole moment and the spatial vector $\mathbf{R}_{12}^0$, the measured PL spectrum is expected to depend on the detector direction (direction of $\mathbf{k}$).

With the analytical solutions of ρ_{c1} and ρ_{c2} (Eqs. (39) and (40)), the stationary solution for the PL spectrum is

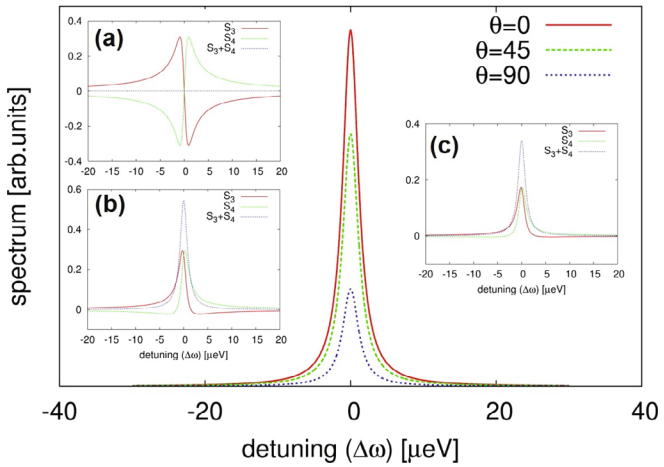

Fig. 7. (Color online) PL spectra of the two coupled QDs for three detector angles. The angle θ is defined by two vectors $\mathbf{R}_2^0$ and $\mathbf{k}$. The third (S_3), the fourth line (S_4) of (49) and $S_3 + S_4$ are plotted as function of $\tilde{\beta}$. $\tilde{\beta} = 0$ for (a), 1.5 μeV for (b) and 3 μeV for (c).

obtained by inserting the formal integration of Eqs. (46) and (47) in Eq. (45):

$$
\begin{aligned}
&S(\omega) \\
&\propto \rho_0 \Bigg[\frac{1-\cos\gamma}{\Delta\omega^2+(\Gamma_2-2\alpha)^2} \left\{ \frac{\Delta\omega^2-\Gamma_2(\Gamma_2-2\alpha)}{\Delta\omega^2+\Gamma_2^2} - \frac{\Gamma_2-2\alpha}{\Gamma_1-2\alpha} \right\} \\
&\quad + \frac{1+\cos\gamma}{\Delta\omega^2+(\Gamma_2+2\alpha)^2} \left\{ \frac{\Delta\omega^2+\Gamma_2(\Gamma_2+2\alpha)}{\Delta\omega^2+\Gamma_2^2} - \frac{\Gamma_2+2\alpha}{\Gamma_1+2\alpha} \right\} \\
&\quad + \frac{\sin\gamma}{(2\tilde{\beta}-\Delta\omega)^2+\Gamma_2^2} \left\{ \frac{\Gamma_1(2\tilde{\beta}-\Delta\omega)+2\tilde{\beta}\Gamma_2}{4\tilde{\beta}^2+\Gamma_1^2} \right. \\
&\qquad \left. - \frac{\Gamma_2(2\tilde{\beta}-\Delta\omega)+\Gamma_2\Delta\omega}{\Delta\omega^2+\Gamma_2^2} \right\} \\
&\quad + \frac{\sin\gamma}{(2\tilde{\beta}+\Delta\omega)^2+\Gamma_2^2} \left\{ \frac{\Gamma_1(2\tilde{\beta}+\Delta\omega)+2\beta\Gamma_2}{4\tilde{\beta}^2+\Gamma_1^2} \right. \\
&\qquad \left. + \frac{-\Gamma_2(2\tilde{\beta}+\Delta\omega)+\Gamma_2\Delta\omega}{\Delta\omega^2+\Gamma_2^2} \right\} \Bigg],
\end{aligned}
\tag{49}
$$

where $\Delta\omega = \nu_k - \tilde{\omega}_g$ and $u_{\mathbf{k}}(\mathbf{R}_2^0) = \cos\gamma + i\sin\gamma$.

The spectrum is decided by four spectral components. While the first two contributions whose peak positions locate at $\omega = \nu_k = \tilde{\omega}_g$ have a narrow $(\Gamma_2 - 2\alpha)$ and a wide full width at half maximum (FWHM) $(\Gamma_2 + 2\alpha)$, respectively, the last two components which have the peaks at $\omega = \tilde{\omega}_g - 2\beta$ and $\omega = \tilde{\omega}_g + 2\beta$, respectively, are featured by the same FWHM Γ_2. However, they are not discriminated in PL spectrum as two distinguishable spectral components.

When the detector is located at a position which is orthogonal with respect to the vector connecting the two QDs ($\mathbf{R}_2^0 \perp \mathbf{k}$), $\cos\gamma = 1$ and $\sin\gamma = 0$, thus, the spectrum is determined only by the second line in Eq. (49). Other three lines can contribute to the spectrum only when the detector begins to be aligned with the direction parallel to the connection vector. In special, the last two spectral components in Eq. (49) are worth examining carefully the contributions to the PL spectrum.

Third and fourth components in Eq. (49) labeled as S_3 and S_4, respectively, and the sum of both are presented in Fig. 7 as insets for three selected values of $\tilde{\beta}$. In the case that $\tilde{\beta} = 0$, S_3 and S_4 compensate exactly each other, leading to zero contribution to the spectrum. If $\tilde{\beta} \neq 0$, they have asymmetric distributions, but the sum of them is a symmetric Lorentzian distribution centered at zero detuning. As a result, PL spectrum measured in a direction parallel to the connection vector ($\theta = 0$) has a most intensive signal as demonstrated in Fig. 7.

We should mention that our finding is a not contradictive result, compared to classical radiation pattern of electric dipoles where the radiation power has the maximum in the direction perpendicular to the dipole polarization direction [48]. In numerical calculations, we assume that the detector located at a constant far-field moves around on xy-plane for the two QDs polarized in z-direction and spatially characterized by $\mathbf{R}_{12}^0$ parallel to x-axis.

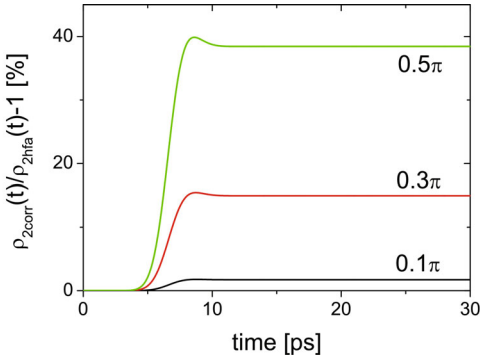

Fig. 8. (Color online) The relative difference of the upper level occupation density of the acceptor QD, calculated by HFA $\rho_{2\mathrm{hfa}}(t)$, with respect to that of the correlation expansion $\rho_{2\mathrm{corr}}(t)$.

3. Validation and break-down of HFA

We finalize this study by discussing the validity and break-down of HFA. The analytical forms of the interband coherences (Eqs. (35) and (36)) and upper level electron densities (Eqs. (39) and (40)) by HFA reproduce exactly the same results (Figs. 4 - 7) obtained from the full correlation expansion of two-electron coherences (exact model).

However, the difference between two approaches begins to increase as the correlation of two electrons, $\langle a_{\kappa 1}^\dagger a_{\lambda 2}^\dagger a_{\mu 2} a_{\nu 1} \rangle^c$, are increased by optically pumped energy. For example, we calculate ρ_2 by full correlation expansion and HFA and denote them as $\rho_{2\mathrm{corr}}$ and $\rho_{2\mathrm{hfa}}$,

respectively. Figure 8 demonstrate the difference of HFA from the exact solution for several values of time-integrated laser pulse area, for which a constant pulse width ($\tau = 50$ fs) and zero radiative decay ($\Gamma_{1/2} = 0$) are simulated. The difference is small enough to be neglected as long as the pulse area is smaller than 0.1π. Therefore, HFA can be applied to study on coherent energy transfer dynamics between QD electrons in linear optical regime.

IV. CONCLUSIONS

In summary, coherent excitation energy transfer between two self-growth semiconductor quantum dots (QDs) was theoretically studied within the framework of Heisenberg's quantum kinetic equations of motion in density matrix formalism. By expanding the reciprocal spatial vector connecting two QDs in the Coulomb interaction Hamiltonian, three diagonal and one off-diagonal coupling matrix elements were derived. We obtained numerical values in the order of a few μeV with eight-band kp-theory wave functions of electron and hole confined in a highly asymmetric pyramidal shape of QD. We also calculated transversal radiation field coupling coefficients, which can give rise to sub- as well as superradiance of both QDs, depending on the initial excitation condition. When only one QD electron is exposed to a weak pump laser field so that the electron remains almost in the lower energy level, all two-electron correlated terms could be replaced by products of two electrons density matrix elements through the Hartree-Fock approximation (HFA). As a results, temporal behaviors of single electronic density matrix elements were derived in fully analytical forms, and the stationary photoluminescence of coupled QDs could be expressed analytically as well. Finally, the validation of the HFA was examined for different values of the time-integrated pump laser pulse area. Our studies presented in this report can contribute to understand coherent excitation energy transfer dynamics between two atomic light emitters and pave the way to realizing devices based on semiconductor QDs for quantum information processing.

Note added – This work partially overlaps with the Ph.D. thesis of the author [49], which has not been published elsewhere as an article.

ACKNOWLEDGMENTS

This work was supported by the National Research Foundation of Korea (NRF) Grants funded by the Korean Government (MSIP) (2018R1A2B6001449).

APPENDIX A: EQUATIONS OF MOTION OF PURELY ELECTRONIC DENSITY MATRIX ELEMENTS

The closed set of Heisenberg's quantum kinetic equations of motion for purely electronic density matrix elements are obtained for the local excitation condition as

$$\begin{aligned}\partial_t p_1 =& -(i\omega_1+\Gamma_{12})p_1 - i\Omega(t)(\rho_{c1}-\rho_{v1})\\ &+ i\{\omega_b\eta_{vvvc}+\omega_c\eta_{vccc}\}\\ &+ \big(i(\beta_2+\omega_F^*)+\alpha_2\big)(\eta_{cvcc}-\eta_{vvcv}),\end{aligned} \tag{A1}$$

$$\begin{aligned}\partial_t\rho_{c1} =& -\Gamma_{11}\rho_{c1} - i\Omega(t)\{p_1-p_1^*\}\\ &+\{-\alpha_2+i(\beta_2+\omega_F)\}\eta_{vcvc}\\ &-\{\alpha_2+i(\beta_2-\omega_F^*)\}\eta_{cvcv},\end{aligned} \tag{A2}$$

$$\begin{aligned}\partial_t p_2 =& -(i\omega_2+\Gamma_{22})p_2 - i\Omega(t)(\rho_{c1}-\rho_{v1})\\ &+ i\{\omega_b\eta_{vvcv}+\omega_c\eta_{cvcc}\}\\ &+ (i(\beta_1+\omega_F)+\alpha_1)(\eta_{vccc}-\eta_{vvvc}),\end{aligned} \tag{A3}$$

$$\begin{aligned}\partial_t\rho_{c2} =& -\Gamma_{21}\rho_{c2} - i\Omega(t)\{p_2-p_2^*\}\\ &-\{\alpha_1+i(\beta_1+\omega_F)\}\eta_{vcvc}\\ &-\{\alpha_1-i(\beta_1+\omega_F^*)\}\eta_{cvcv},\end{aligned} \tag{A4}$$

$$\partial_t\eta_{vvvv} = -i\Omega(t)\big\{\eta_{cvvv}-\eta_{vvvc}+\eta_{vcvv}-\eta_{vvcv}\big\}, \tag{A5}$$

$$\begin{aligned}\partial_t\eta_{vvcv} =& \big\{-i\omega_2-\Gamma_{22}+i\omega_b\big\}\eta_{vvcv}\\ &-\Big\{i(\beta_2+\omega_F)+\alpha_2\Big\}\eta_{vvvc}\\ &-i\Omega(t)\big\{\eta_{cvcv}-\eta_{vvcc}+\eta_{vccv}-\eta_{vvvv}\big\}\\ =&\partial_t\eta^*_{vcvv},\end{aligned} \tag{A6}$$

$$\begin{aligned}\partial_t\eta_{vccv} =& -\Gamma_{21}\eta_{vccv} - \{\alpha_1+i(\beta_1+\omega_F)\}\eta_{vcvc}\\ &-\{\alpha_1-i(\beta_1+\omega_F^*)\}\eta_{cvcv}\\ &-i\Omega(t)\big\{\eta_{cccv}-\eta_{vccc}+\eta_{vvcv}-\eta_{vcvv}\big\},\end{aligned} \tag{A7}$$

$$\begin{aligned}\partial_t\eta_{vvvc} =& \big\{-i\omega_1-\Gamma_{12}+i\omega_b\big\}\eta_{vvvc}\\ &-\{i(\beta_2+\omega_F^*)+\alpha_2\}\eta_{vvcv}\\ &-i\Omega(t)\big\{\eta_{cvvc}-\eta_{vvvv}+\eta_{vcvc}-\eta_{vvcc}\big\}\\ &=\partial_t\eta^*_{cvvv},\end{aligned} \tag{A8}$$

$$\begin{aligned}\partial_t\eta_{vvcc} =& \big\{-i(\omega_1+\omega_2)-\Gamma_{12}-\Gamma_{22}+i\omega_b\big\}\eta_{vvcc}\\ &-i\Omega(t)\big\{\eta_{cvcc}-\eta_{vvcv}+\eta_{vccc}-\eta_{vvvc}\big\}\\ &=\partial_t\eta^*_{ccvv},\end{aligned} \tag{A9}$$

$$\begin{aligned}\partial_t\eta_{vcvc} =& \big\{-i(\omega_1-\omega_2)-\Gamma_{12}-\Gamma_{22}\big\}\eta_{vcvc}\\ &-\{\alpha_1-i(\beta_1+\omega_F^*)\}\eta_{cvvc}\\ &-\{\alpha_2+i(\beta_2+\omega_F^*)\}\eta_{vccv}\\ &-i\Omega(t)\big\{\eta_{ccvc}-\eta_{vcvv}+\eta_{vvvc}-\eta_{vccc}\big\}\\ &=\partial_t\eta^*_{cvcv},\end{aligned} \tag{A10}$$

$$\begin{aligned}\partial_t\eta_{vccc} =& \big\{-i\omega_1-\Gamma_{12}-\Gamma_{21}+i\omega_c\big\}\eta_{vccc}\\ &+\{i(\beta_1+\omega_F^*)-\alpha_1\}\eta_{cvcc}\\ &-i\Omega(t)\{\eta_{cccc}-\eta_{vccv}+\eta_{vvcc}-\eta_{vcvc}\}\\ &=\partial_t\eta^*_{cccv},\end{aligned} \tag{A11}$$

$$\begin{aligned}\partial_t\eta_{cvvc} =& -\Gamma_{11}\eta_{cvvc} - \{\alpha_2 + i(\beta_2 - \omega_F)\}\,\eta_{vcvc} \\ & - \{\alpha_2 - i(\beta_2 + \omega_F^*)\}\,\eta_{cvcv} \\ & - i\Omega(t)\big\{\eta_{vvvc} - \eta_{cvvv} + \eta_{ccvc} - \eta_{cvcc}\big\},\end{aligned} \tag{A12}$$

$$\begin{aligned}\partial_t\eta_{cvcc} =& \big\{ -i\omega_2 - \Gamma_{11} - \Gamma_{22} + i\omega_c\big\}\eta_{cvcc} \\ & + \{i(\beta_1 + \omega_F) - \alpha_1\}\,\eta_{vccc} \\ & - i\Omega(t)\big\{\eta_{vvcc} - \eta_{cvcv} + \eta_{cccc} - \eta_{cvvc}\big\} \\ & = \partial_t\eta^*_{ccvc},\end{aligned} \tag{A13}$$

$$\begin{aligned}\partial_t\eta_{cccc} =& -(\Gamma_{11} + \Gamma_{21})\eta_{cccc} \\ & - i\Omega(t)\big\{\eta_{vccc} - \eta_{cccv} + \eta_{cvcc} - \eta_{ccvc}\big\},\end{aligned} \tag{A14}$$

REFERENCES

[1] D. Bimberg, ed., *Semiconductor Nanostructures, Nanoscience and technology* (Springer, Berlin, 2008).

[2] P. Borri, W. Langbein, S. Schneider, U. Woggon, R. L. Sellin, D. Quyang and D. Bimberg, Phys. Rev. Lett. **87**, 157401 (2001).

[3] P. Borri, W. Langbein, U. Woggon, M. Schwab, M. Bayer, S. Fafard, Z. Wasilewski and P. Hawrylak, Phys. Rev. Lett. **91**, 267401 (2003).

[4] M. Bayer, P. Hawrylak, K. Hinzer, S. Fafard, M. Korkusinski, Z. R. Wasilewski, O. Sterna and A. Forchel, Science **291**, 451 (2001).

[5] E. Biolatti, I. D'Amico, P. Zanardi and F. Rossi, Phys. Rev. B **65**, 075306 (2002).

[6] B. W. Lovett, J. H. Reina, A. Nazir, G. Andrew and D. Briggs, Phys. Rev. B **68**, 205319 (2003).

[7] J. P. Reithmaier, G. Sek, A. Löffler, C. Hofmann, S. Kuhn, S. Reitzenstein, L. V. Keldysh, V. D. Kulakovskii, T. L. Reinecke and A. Forchel, nature **432**, 197 (2004).

[8] A. Nazir, B. W. Lovett, S. D. Barrett, J. H. Reina, G. Andrew and D. Briggs, Phys. Rev. B **71**, 045334 (2005).

[9] K. Becker, J. M. Lupton, J. Müller, A. L. Rogach, D. V. Talapin, H. Weller and J. Feldmann, Nature Materials **5**, 777 (2006), URL http://dx.doi.org/10.1038/nmat1738.

[10] T. Frey, P. J. Leek, M. Beck, A. Blais, T. Ihn, K. Ensslin and A. Wallraff, Phys. Rev. Lett. **108**, 046807 (2012), URL https://link.aps.org/doi/10.1103/PhysRevLett.108.046807.

[11] P. Michler, ed., *Quantum Dots for Quantum Information Technologies, Nano-Optics and Nanophotonics* (Springer, Berlin, 2017).

[12] G. Ortner, M. Bayer, Y. Lyanda-Geller, T. L. Reinecke, A. Kress, J. P. Reithmaier and A. Forchel, Phys. Rev. Lett. **94**, 157401 (2005).

[13] T. Förster, Discuss. Faraday. Soc. **27**, 7 (1959).

[14] J. Danckwerts, K. J. Ahn, J. Förstner, and A. Knorr, Phys. Rev. B **73**, 165318 (2006), URL https://link.aps.org/doi/10.1103/PhysRevB.73.165318.

[15] S. Jang, Y-C. Cheng, D. R. Reichman and J. D. Eaves, The Journal of Chemical Physics **129**, 101104 (2008), URL https://doi.org/10.1063/1.2977974.

[16] D. Kim, S. Okahara, M. Nakayama and Y. Shim, Phys. Rev. B **78**, 153301 (2008), URL https://link.aps.org/doi/10.1103/PhysRevB.78.153301.

[17] G. Parascandolo and V. Savona, Phys. Rev. B **71**, 045335 (2005).

[18] P. W. Milonni and P. L. Knight, Phys. Rev. A **10**, 1096 (1974).

[19] P. W. Milonni and P. L. Knight, Phys. Rev. A **11**, 1090 (1975).

[20] M. J. Stephen, J. Chem. Phys. **40**, 669 (1964).

[21] P. R. Fontana and D. D. Hearn, Phys. Rev. Lett. **19**, 481 (1967).

[22] J. Förstner, K. J. Ahn, J. Danckwerts, M. Schaarschmidt, I. Waldmüller, C. Weber and A. Knorr, Phys. Stat. Sol. (b) **234**, 155 (2002).

[23] J. Förstner, C. Weber, J. Danckwerts and A. Knorr, Phys. Rev. Lett. **91**, 127401 (2003).

[24] B. Krummheuer, V. M. Axt and T. Kuhn, Phys. Rev. B **65**, 195313 (2002).

[25] J. Förstner, C. Weber, J. Danckwerts and A. Knorr, phys. stat. sol. (b) **238**, 419 (2003).

[26] K. J. Ahn, J. Förstner and A. Knorr, Phys. Rev. B **71**, 153309 (2005).

[27] E. Rozbicki and P. Machnikowski, Phys. Rev. Lett. **100**, 027401 (2008), URL https://link.aps.org/doi/10.1103/PhysRevLett.100.027401.

[28] K. J. Ahn and A. Knorr, Phys. Rev. B **68**, 161307(R) (2003).

[29] J-Q. Liao, J-F. Huang, L-M. Kuang and C. P. Sun, Phys. Rev. A **82**, 052109 (2010), URL https://link.aps.org/doi/10.1103/PhysRevA.82.052109.

[30] M. Bayer, T. L. Reinecke, F. Weidner, A. Larionov, A. McDonald and A. Forchel, Phys. Rev. Lett. **86**, 3168 (2001).

[31] S. Hughes, Phys. Rev. Lett. **94**, 227402 (2005).

[32] F. Reil, U. Hohenester, J. R. Krenn and A. Leitner, Nano Lett. **8**, 4128 (2008), URL https://doi.org/10.1021/nl801480m.

[33] V. K. Komarala, A. L. Bradley, Y. P. Rakovich, S. J. Byrne, Y. K. Gun'ko, and A. L. Rogach, Applied Physics Letters **93**, 123102 (2008), https://doi.org/10.1063/1.2981209, URL https://doi.org//10.10631.2981209.

[34] O. Stier, M. Grundmann and D. Bimberg, Phys. Rev. B **59**, 5688 (1999).

[35] M. O. Scully and M. S. Zubairy, *Quantum Optics* (Cambridge University Press, Cambridge, 1997).

[36] J. M. Gerton, L. A. Wade, G. A. Lessard, Z. Ma and S. R. Quake, Phys. Rev. Lett. **93**, 180801 (2004).

[37] G. D. Mahan, *Many-Particle Physics* (Plenum Press, New York, 1981).

[38] M. Winkelnkemper, A. Schliwa and D. Bimberg, Phys. Rev. B **74**, 155322 (2006), URL https://link.aps.org/doi/10.1103/PhysRevB.74.155322.

[39] A. Schliwa, M. Winkelnkemper and D. Bimberg, Phys. Rev. B **76**, 205324 (2007), URL https://link.aps.org/doi/10.1103/PhysRevB.76.205324.

[40] S. Rodt, R. Heitz, A. Schliwa, R. L. Sellin, F. Guffarth and D. Bimberg, Phys. Rev. B **68**, 035331 (2003).

[41] O. Stier, Ph.D. thesis, Technical University Berlin, 2000.

[42] L. Allen and J. H. Eberly, *Optical Resonance and Two-Level System* (Dover Publications, INC., New York, 1987).

[43] G. S. Agarwal, *Quantum Statistical Theories of Spontaneous Emission and Their Relation to Other Approach* (Springer, Berlin, 1974).

[44] H. Freedhoff, Phys. Rev. A **69**, 013814 (2004).
[45] G. B. Arfken and H. J. Weber, *Mathematical Methods for Physicists* (Harcourt Academic, London, 2001).
[46] K. J. Ahn, F. Milde and A. Knorr, Phys. Rev. Lett. **98**, 027401 (2007), URL https://link.aps.org/doi/10.1103/PhysRevLett.98.027401.
[47] K. J. Ahn, J. Korean Phys. Soc. **71**, 657 (2017), URL https://doi.org/10.3938/jkps.71.722.
[48] J. D. Jackson, *Classical Electrodynamics* (John Wiley & Sons, Inc., New York, 1999), 3rd ed.
[49] K. J. Ahn, Ph.D. thesis, Technische Universität Berlin, 2006.